

RM AOI Algorithm Development of FPCB Bending for Zero Bezel Flexible OLED

Kyunghan Chun^a

^aDepartment of Electronic Engineering, Daegu Catholic University, Gyeongbuk, Korea

^akchun@cu.ac.kr

Abstract: In this paper, we propose an RM(radius measurement) AOI(automatic optical inspection) method to determine the suitability of the FPCB(flexible printed circuit board) bending process for zero bezel OLED(organic light emitting diode). Recently, OLED has become the mainstream of mobile displays, and it is possible to realize a flexible display that can flexibly bend the screen. In particular, in order to increase the size of these displays, the zero bezel technology that reduces the bezel as much as possible is attracting attention. Mass production and quality uniformity are required through AOI inspection after bending. We develop an algorithm for RM AOI, apply non-linear optimization to improve inspection performance, and verify through experiments.

Keywords: AOI, optimization, FPCB, OLED, bending

1. Introduction

In modern factories, and in factories of the future, much more will be done by autonomous machines using visual feedback [1]. Visual feedback can be used to navigate the workspace, avoid obstacles, and identify and locate parts. Standard area scan cameras and RGB cameras in various vision technologies such as structured lighting, time-of-flight and laser triangulation, line can cameras, stereo vision and monocular vision are widely used in the industry for inspection and quality control processes[2], [3]. And many advanced quality inspection methods have been proposed, including deep learning methods [4].

Automated visual inspection is one of the innovations for machine development. These systems are widely used in industrial applications such as identification[5] of industrial instruments, measurement, classification of objects[6], automatic inspection[7], rejects[8] or tools. This helps the system to maintain the best accuracy performance [9], reliable [10] and low cost with the results obtained in real time. Image processing innovations are faster and require no human monitoring [11-12].

In this paper, for the manufacture of Zero Bezel smartphone employing flexible OLED, we develop an algorithm to determine the curvature test after automated bending of FPCB. The inspection process, which was performed manually, requires AOI especially for the automated process. It implements inspection (RM, Radius Measurement) of acceptance through AOI of these bending results and improves measurement performance through optimization.

2. FPCB Bending for Zero Bezel OLED

With the recent changes in OLED, it has become the mainstream of mobile displays with excellent picture quality, thin thickness, and light weight, and it is possible to implement flexible displays that can flexibly bend the screen. Existing displays, such as liquid crystal displays (LCDs), are very difficult to bend, fold, roll, or even stretch like fibers.

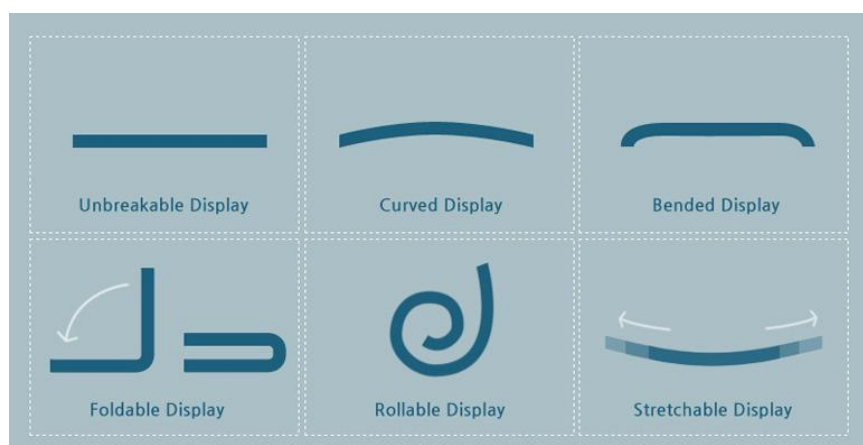


Figure 1. Various form factor [13]

Traditional OLEDs are called rigid OLEDs. The reason why it is hard is that the lower substrate of the display and the encapsulating material that plays a protective role are glass. The so-called form factor innovation that freely implements the form of mobile devices such as smartphones is difficult to implement with rigid OLEDs. A technology that uses Flexible OLED to round both the left and right sides of the device with a steep edge has been developed. In addition to this flexible OLED, in particular, Zero Bezel technology, which reduces the bezel as much as possible to increase the size of the display, is in the spotlight.

In order to manufacture a Zero Bezel smartphone employing flexible OLED, it is necessary to develop a device that can automatically bend FPCB, which was previously performed manually. In this case, the radius should be 0.3mm or less and it is important to minimize the curvature below 0.3mm. Inspection (RM, Radius Measurement) of these bending results through AOI is a necessary process for mass production and quality uniformity.

The FPCB bending machine used in this paper is as follows.

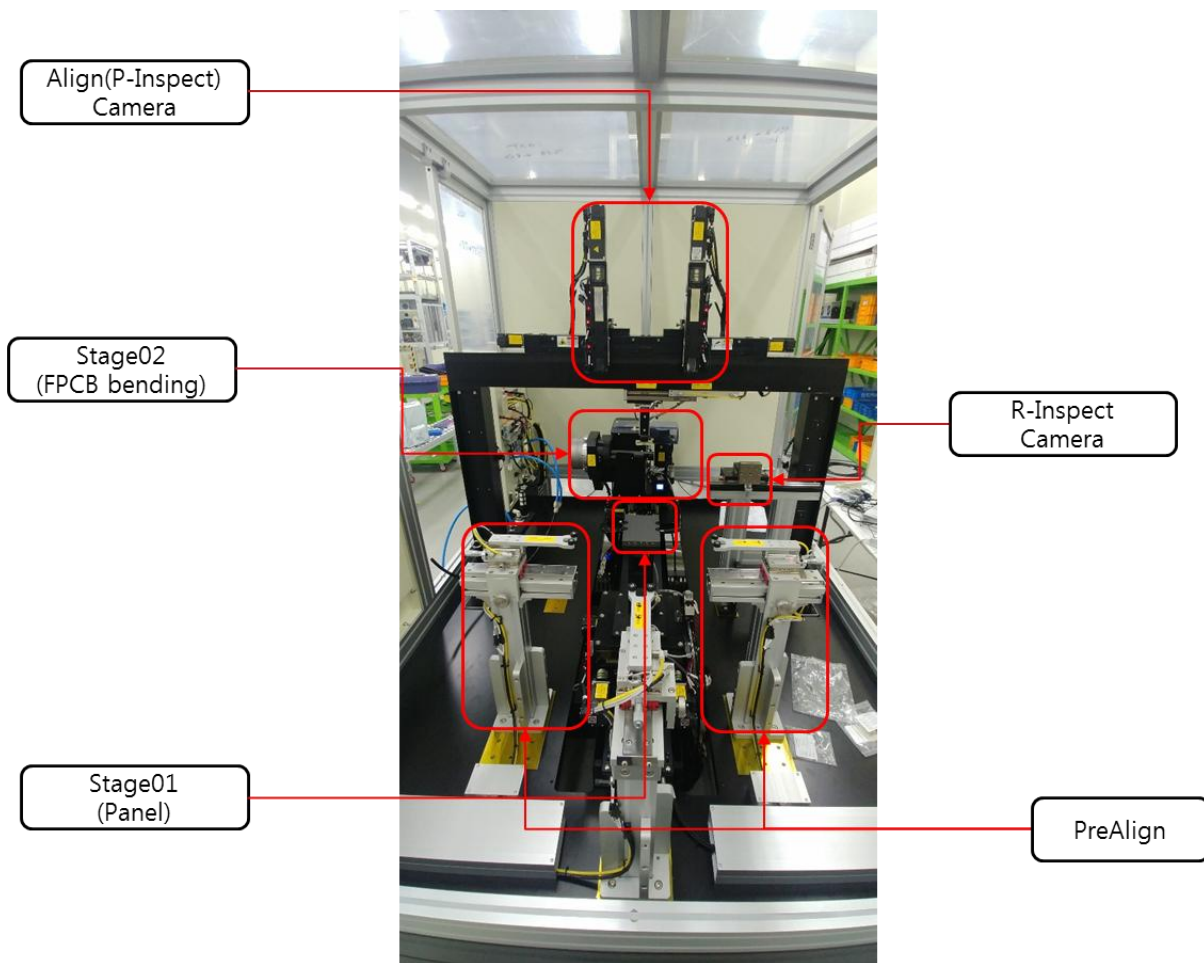


Figure 2.FPCB bending machine

There are a camera for positioning in 12 o'clock direction. The camera for curvature measurement AOI is located in the 3 o'clock direction, and when the object moves to the reference position in stage01, bending is performed in stage02. This equipment is applied to the tab process in the OLED manufacturing, which is a facility that automatically bends the FPCB attached and a camera in 3 o'clock direction decides the production quality in the tab process.

The tab process during the OLED manufacturing is performed after four steps (1. glass inspection, 2. photo/TFT (Thin Film Transistor) process, 3. evaporation process, and 4. aging process), and RM AOI inspection is performed after bending in the tab process.

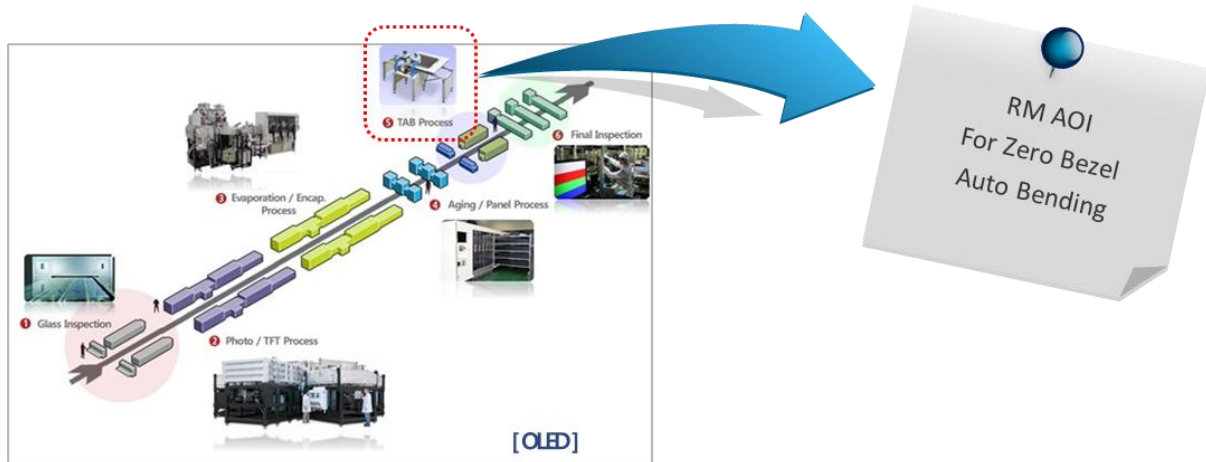


Figure 3.OLED manufacture

3. RM AOI Algorithm

For bending, first, the FPCB is closely attached to the pad by vacuum, and when the spindle equipped with the vacuum pad fixture rotates slowly based on the bending center A, the FPCB contacts the round bar at point C. When contact with the round bar starts, in order to minimize the phenomenon that the round bar is pushed in the X-axis direction, the bending operation is performed along the circumference of the round bar at point f as bending proceeds along the circumference of the round bar while reducing the feed angular velocity of the X axis to the maximum. At this time, the FPCB is attached to the FPD (flat panel display) Panel.

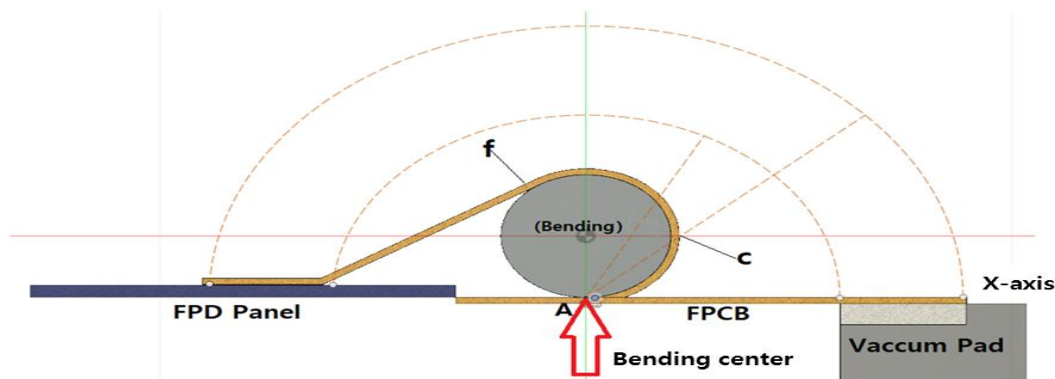


Figure 4.Bending

For product recognition and radius measurement in the camera image, first, after recognizing the side of the product, the point that meets the leftmost point of the x-axis from the reference point (center) is defined as A, and the points that meet below and above the y-axis are defined as B and C, respectively, to define a triangle.

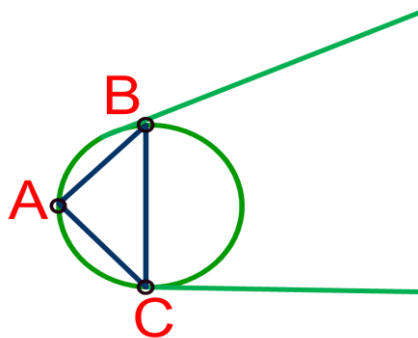


Figure 5.Side view of FPCB after bending

The reason to make a triangle by recognizing the three points is to measure the radius of curvature using the principle of geometry because there is no guarantee that the result will be an accurate circle even if it is bent to make a circle. The radius of curvature can be calculated by finding the radius of the circumscribed circle using the completed triangle.

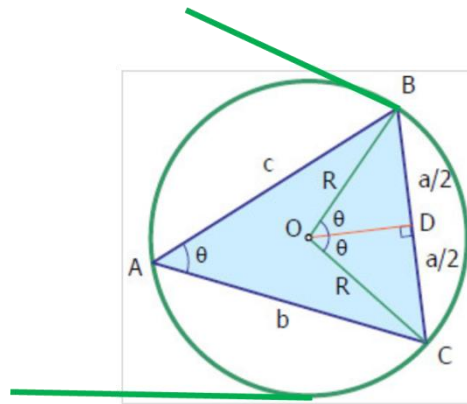


Figure 6. Radius of the circumscribed circle

$$R = \frac{abc}{4\text{area}} = \frac{|\vec{a}||\vec{b}||\vec{c}|}{2|\vec{a} \times \vec{b}|} \tag{1}$$

The algorithm used to calculate the radius of curvature is as follows.

```
#define SQR(x) ((x)*(x))
doublecircumradius(CPoint A, CPoint B, CPoint C){
    doubleax=C.x-B.x;
    double ay=C.y-B.y;
    doublebx=A.x-C.x;
    double by=A.y-C.y;
    doublecrossab=ax*by-ay*bx;
    if(crossab!=0){
        double a=sqrt(SQR(ax)+SQR(ay));
        double b=sqrt(SQR(bx)+SQR(by));
        double cx=B.x-A.x;
        double cy=B.y-A.y;
        double c=sqrt(SQR(cx)+SQR(cy));
        return(0.5*a*b*c/fabs(crossab));
    }
    else
        return(-1.0); // -1 means computation failure
}
```

The center point recognition acts as an important factor in calculating the radius of curvature. For this, we use aligned center point-based recognition and automatic center point recognition method. First, the aligned center point-based recognition method is determined by extracting the curved surface and intersection point of the product in each direction based on a fixed seed (point). This can be seen as applicable because the real bending process includes a pre-aligned step.

```
Point p1 = new Point(1000, 270),
```

```
p2 = new Point(500, 570),
p3 = new Point(500, 0);
```

On the other hand, with automatic center point recognition, the center point is determined by recognizing the product side edge and generating an appropriate seed (point) based on the extracted center point and extracting the intersection point with the curved surface of the product in each direction.

```
foreach (Point[] p in new_contours)
{
    Moments moments = Cv2.Moments(p, false);
    cx = (int)(moments.M10 / moments.M00);
    cy = (int)(moments.M01 / moments.M00);
}
Point p1 = new Point(cx-50, cy),
p2 = new Point(cx, cy-50),
p3 = new Point(cx, cy+50);
```

As a result of measuring the radius in the test bed by using an image, the measured value shows an error between the actual values and tends to increase gradually.

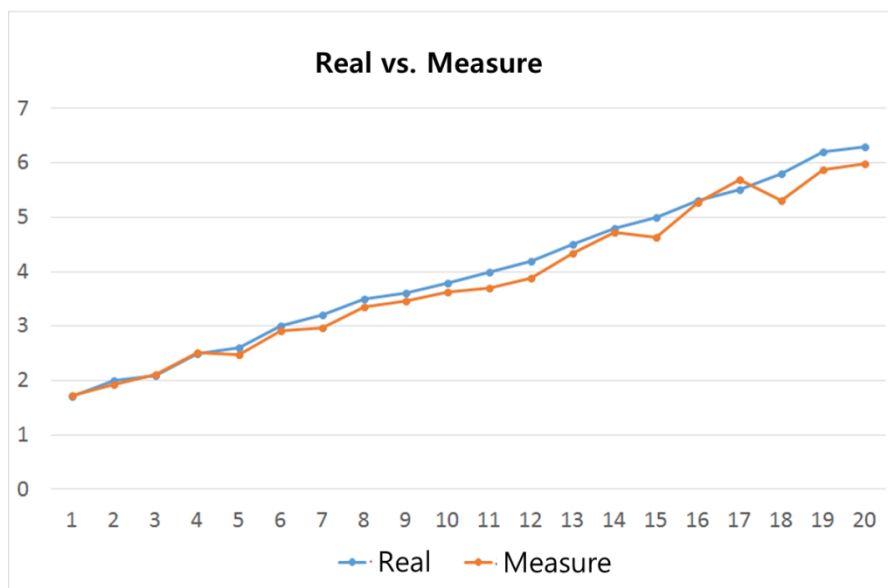


Figure 7. Real value vs. Measure value

In order to solve this problem, the error can be improved and the measurement performance can be improved by applying the linear compensation method. And if the increasing tendency is non-linear, the non-linear error improvement is applied by applying the segmented linear compensation method. Finally, in order to optimize the linear and non-linear compensation methods, LS(least square) is applied to obtain an optimized parameter value based on the measured values.

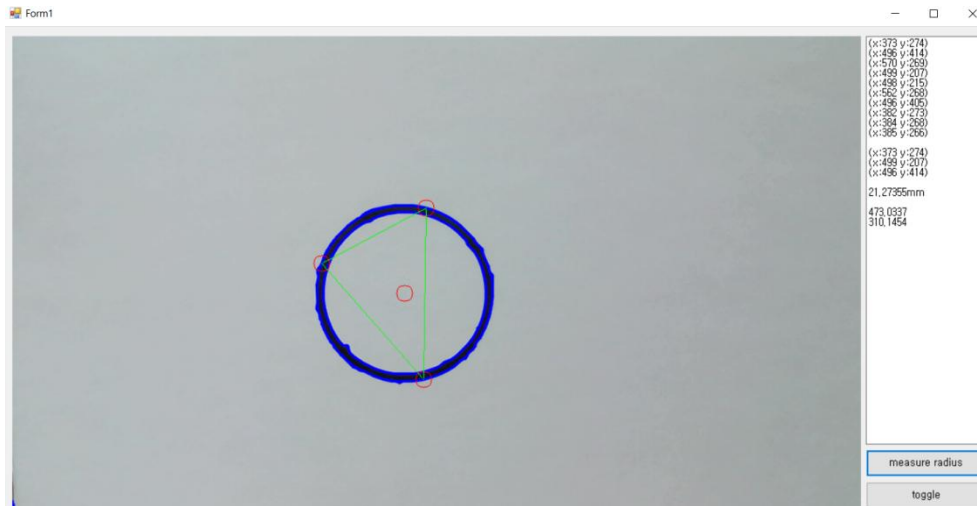
$$a = \frac{\sum_{i=1}^n (y_i - \bar{y})(x_i - \bar{x})}{\sum_{i=1}^n (x_i - \bar{x})^2}, \quad b = \bar{y} - a\bar{x} \tag{2}$$

where \bar{y} is the average of the actual values, and \bar{x} is the average of the measured values.

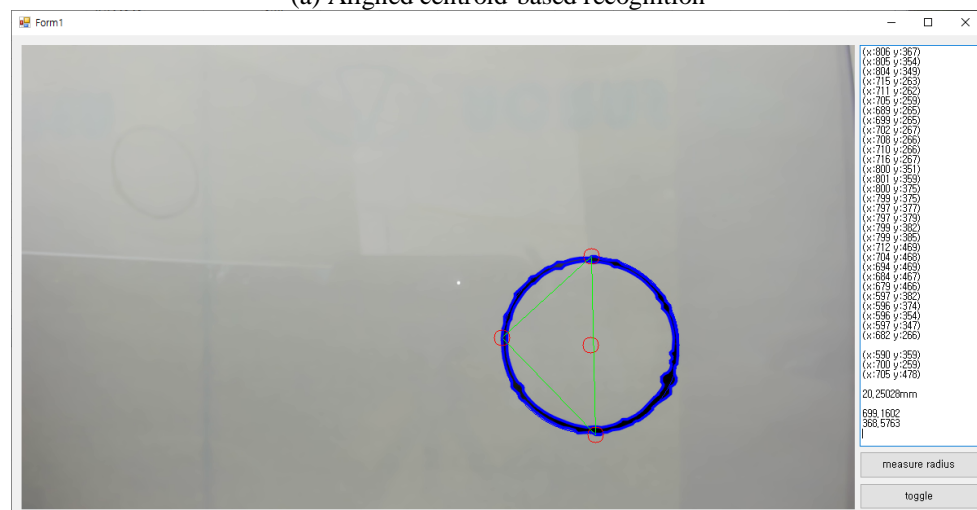
4. Test and Validation

In this paper, product image recognition and radius of curvature measurement were tested in a test bed. The test system recognized the edge of the product using a camera and applied an algorithm for measuring the radius of a triangular circumscribed circle based on three points extracted from the recognition curve.

First, it is a center point recognition test, which is a standard for measuring the radius of curvature. The aligned center point-based recognition and automatic center point recognition methods are as follows.



(a) Aligned centroid-based recognition



(b) Automatic center point recognition

Figure 8.Center point recognition

To examine the improvement results after compensation in the test system using AOI equipment, AOI improvement using the linear compensation method is as follows. A linear compensation method ($y = ax$) was applied to fix the measurement error by the camera, and the results were compared with the sum of the error squares.

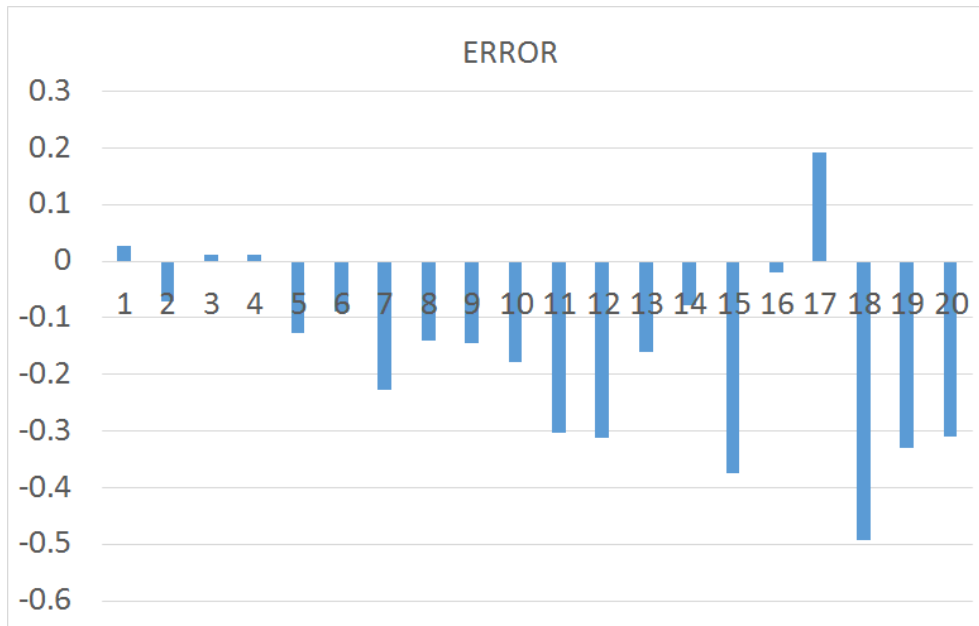


Figure 11. Linear compensation error

To confirm a more accurate value, it can be seen that the value increases more than twice based on 10 in Figure 11. From this, the AOI improvement method using the non-linear compensation method compensates by a segmented linear method in which compensation of a different slope is applied to each segment, which can be applied by dividing an appropriate section and setting a different slope for each section.

	A	B	C	D	E	F	G	H	I	J
1	1.7	1.726	0.026	0.1	1.76052	0.06052	0.003663	1.62244	-0.07756	0.006016
2	2	1.928	-0.072	0.1	1.96656	-0.03344	0.001118	1.81232	-0.18768	0.035224
3	2.1	2.112	0.012	0.1	2.15424	0.05424	0.002942	1.98528	-0.11472	0.013161
4	2.5	2.512	0.012	0.2	2.56224	0.06224	0.003874	2.36128	-0.13872	0.019243
5	2.6	2.472	-0.128	0.2	2.52144	-0.07856	0.006172	2.32368	-0.27632	0.076353
6	3	2.91	-0.09	0.1	2.9682	-0.0318	0.001011	2.7354	-0.2646	0.070013
7	3.2	2.972	-0.228	0.1	3.03144	-0.16856	0.028412	2.79368	-0.40632	0.165096
8	3.5	3.36	-0.14	0.1	3.4272	-0.0728	0.0053	3.1584	-0.3416	0.116691
9	3.6	3.456	-0.144	0.1	3.66336	0.06336	0.004014	4.11264	0.51264	0.2628
10	3.8	3.621	-0.179	0.1	3.83826	0.03826	0.001464	4.30899	0.50899	0.259071
11	4	3.696	-0.304	0.2	3.91776	-0.08224	0.006763	4.39824	0.39824	0.158595
12	4.2	3.887	-0.313	0.1	4.12022	-0.07978	0.006365	4.62553	0.42553	0.181076
13	4.5	4.34	-0.16	0.1	4.6004	0.1004	0.01008	5.1646	0.6646	0.441693
14	4.8	4.723	-0.077	0.1	5.00638	0.20638	0.042593	5.62037	0.82037	0.673007
15	5	4.626	-0.374	0.2	4.90356	-0.09644	0.009301	5.50494	0.50494	0.254964
16	5.3	5.28	-0.02	0.1	5.5968	0.2968	0.08809	6.2832	0.9832	0.966682
17	5.5	5.691	0.191	0.1	6.03246	0.53246	0.283514	6.77229	1.27229	1.618722
18	5.8	5.308	-0.492	0.1	5.62648	-0.17352	0.030109	6.31652	0.51652	0.266793
19	6.2	5.87	-0.33	0.1	6.2222	0.0222	0.000493	6.9853	0.7853	0.616696
20	6.3	5.991	-0.309	0.1	6.35046	0.05046	0.002546	7.12929	0.82929	0.687722
21							0.537824			6.889617
22							Sum of squared error			Sum of squared error

Figure 12. Nonlinear compensation data

Divide into two sections, 1-9 and 10-20, and apply linear compensation for each section by determining each slope. It is the result of compensating for nonlinear E by 1.02/1.06 and for nonlinear H by 0.94/1.19 in Figure 12. As a result, it can be confirmed that the sum of squared errors of nonlinear E is smaller than H.

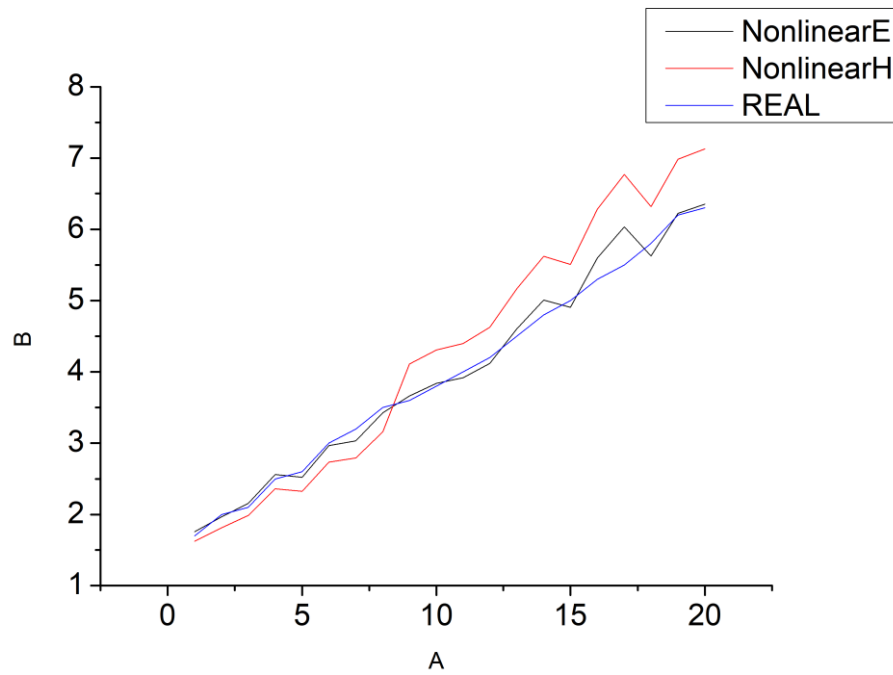


Figure 13. Nonlinear compensation result

For more optimized measurement, the values of a and b that minimize the sum of squared errors of $y = ax + b$ are calculated using Eq. 2 based on the given measurement data by applying the LS algorithm. This is applied to linear and non-linear compensation to select an optimal solution and compare the results. First, the optimal solutions for each method are found as follows.

A	B	C	D	E	F	G	H	I	J	K	
			Linear								
1.7	1.726		-2.09805	4.401814			-2.28	-2.09805	4.783554	1.043901 a	
2	1.928		-1.89605	3.595006			-1.98	-1.89605	3.754179	-0.01193 b	
2.1	2.112		-1.71205	2.931115			-1.88	-1.71205	3.218654		
2.5	2.512		-1.31205	1.721475			-1.48	-1.31205	1.941834		
2.6	2.472		-1.35205	1.828039			-1.38	-1.35205	1.865829		
3	2.91		-0.91405	0.835487			-0.98	-0.91405	0.895769		
3.2	2.972		-0.85205	0.725989			-0.78	-0.85205	0.664599		
3.5	3.36		-0.46405	0.215342			-0.48	-0.46405	0.222744		
3.6	3.456		-0.36805	0.135461			-0.38	-0.36805	0.139859		
3.8	3.621		-0.20305	0.041229			-0.18	-0.20305	0.036549		
4	3.696		-0.12805	0.016397			0.02	-0.12805	-0.00256		
4.2	3.887		0.06295	0.003963			0.22	0.06295	0.013849		
4.5	4.34		0.51595	0.266204			0.52	0.51595	0.268294		
4.8	4.723		0.89895	0.808111			0.82	0.89895	0.737139		
5	4.626		0.80195	0.643124			1.02	0.80195	0.817989		
5.3	5.28		1.45595	2.11979			1.32	1.45595	1.921854		
5.5	5.691		1.86695	3.485502			1.52	1.86695	2.837764		
5.8	5.308		1.48395	2.202108			1.82	1.48395	2.700789		
6.2	5.87		2.04595	4.185911			2.22	2.04595	4.542009		
6.3	5.991		2.16695	4.695672			2.32	2.16695	5.027324		
3.98	3.82405			34.85774					36.38802		
y bar	x bar										

(a) Optimized linear compensation parameters

M	N	O	P	Q	R	S	T	U	V	
			Nonlinear							
1.7	1.726		-0.87933	0.773227	-0.98889	-0.87933	0.869563	1.100333 a		
2	1.928		-0.67733	0.45878	-0.68889	-0.67733	0.466607	-0.17785		
2.1	2.112		-0.49333	0.243377	-0.58889	-0.49333	0.290518			
2.5	2.512		-0.09333	0.008711	-0.18889	-0.09333	0.01763			
2.6	2.472		-0.13333	0.017778	-0.08889	-0.13333	0.011852			
3	2.91		0.304667	0.092822	0.311111	0.304667	0.094785			
3.2	2.972		0.366667	0.134445	0.511111	0.366667	0.187408			
3.5	3.36		0.754667	0.569522	0.811111	0.754667	0.612119			
3.6	3.456		0.850667	0.723634	0.911111	0.850667	0.775052			
2.688889	2.605333			3.022296			3.325533			
y bar	x bar									
3.8	3.621		-1.20018	1.440437	-1.23636	-1.20018	1.483862	0.971226 a		
4	3.696		-1.12518	1.266035	-1.03636	-1.12518	1.166098	0.353904		
4.2	3.887		-0.93418	0.872696	-0.83636	-0.93418	0.781316			
4.5	4.34		-0.48118	0.231536	-0.53636	-0.48118	0.258089			
4.8	4.723		-0.09818	0.00964	-0.23636	-0.09818	0.023207			
5	4.626		-0.19518	0.038096	-0.03636	-0.19518	0.007098			
5.3	5.28		0.458818	0.210514	0.263636	0.458818	0.120961			
5.5	5.691		0.869818	0.756583	0.463636	0.869818	0.403279			
5.8	5.308		0.486818	0.236992	0.763636	0.486818	0.371752			
6.2	5.87		1.048818	1.100019	1.163636	1.048818	1.220442			
6.3	5.991		1.169818	1.368474	1.263636	1.169818	1.478224			
5.036364	4.821182			7.531022			7.314327			
ybar	xbar									

(b) Optimized nonlinear compensation parameters

Figure 14.LS optimization

The *a* and *b* values obtained by applying LS to the linear method are 1.043901 and -0.01193. In the case of the nonlinear method, the *a* and *b* values of section 1 (1-9) are 1.100333, -0.17785, and section 2 (10-20) is 0.971266, 0.353904. When the sum of squared errors of the two methods is calculated, the linearity is about 0.45 and the nonlinearity is 0.39, which shows that the nonlinear method has the least sum of squares error. These values show that the result using LS reduces the sum of squared errors compared to the case where it is not, and it can be seen that more optimization is possible in nonlinearity than in linearity.

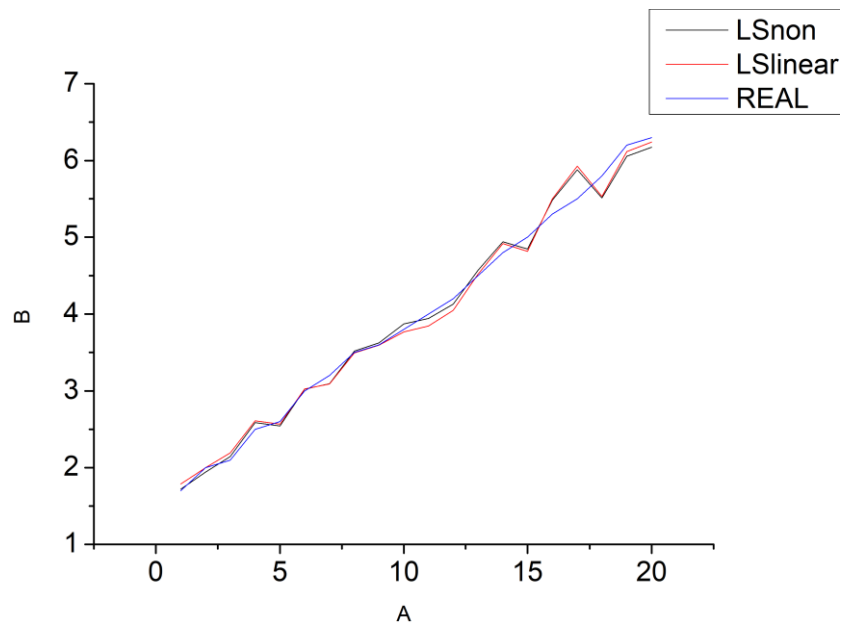


Figure 15.Optimized compensation by LS

5. Conclusion

In this paper, we propose a radius measurement AOI method to determine the suitability of the FPCB bending process and a method for optimizing it. The computer vision system recognizes the side edge of the product, measures the radius of curvature, and analyzes it to determine the quality of the product. By applying linear and non-linear compensation methods to these tests, the measurement performance is improved and, in particular, LS is used to optimize it. When implementing the compensation method, the difference in the degree of error compensation of the measurement position is checked based on the error characteristics according to the characteristics of the lens.

ACKNOWLEDGMENT

This work was supported by research grants from the Daegu Catholic University in 2020.

References

- [1] Ministry of Trade, Industry and Energy, Renewable energy 3020 implementation plan, Rep. of Korea, Feb. 2017.
- [2] A. G. Tsikalakis and N. D. Hatziargyriou, "Centralized control for optimizing microgrids operation," *IEEE Trans. Energy Conv.*, vol. 23, no. 1, pp. 241–248, Feb. 2008.
- [3] S. A. Pourmousavi, M. H. Nehrir, C. M. Colson, and C. Wang, "Realtime energy management of a stand-alone hybrid wind-microturbine energy system using particle swarm optimization," *IEEE Trans. Sustain. Energy*, vol. 1, no. 3, pp. 193–201, Oct. 2010.
- [4] F. A. Mohamed and H. N. Kovio, "Power management strategy for solving power dispatch problems in MicroGrid for residential applications," in *Proc. IEEE Int. Energy Conf. Exhibit.*, Manama, Bahrain, 2010, pp. 746–751.
- [5] Y. Riffonneau, S. Bacha, F. Barruel, and S. Ploix, "Optimal power flow management for grid connected PV systems with batteries," *IEEE Trans. Sustain. Energy*, vol. 2, no. 3, pp. 309–320, Feb. 2011.
- [6] B. Belvedere et al., "A microcontroller-based power management system for standalone microgrids with hybrid power supply," *IEEE Trans. SmartGrid*, vol. 3, no. 3, pp. 422–431, May 2012.
- [7] S. A. Pourmousavi, R. K. Sharma, and B. Asghari, "A framework for real-time power management of a grid-tied microgrid to extend battery lifetime and reduce cost of energy," in *Proc. IEEE PES Innov. SmartGrid Technol.*, Washington, DC, USA, 2012, pp. 1–8.
- [8] C. M. Colson and M. H. Nehrir, "Comprehensive real-time microgrid power management and control with distributed agents," *IEEE Trans. Smart Grid*, vol. 4, no. 1, pp. 617–627, Jan. 2013.
- [9] C. Colson, M. H. Nehrir, R. K. Sharma, and B. Asghari, "Improving sustainability of hybrid energy systems part II: Managing multiple objectives with a multiagent system," *IEEE Trans. Sustain. Energy*, vol. 5, no. 1, pp. 46–54, Jan. 2014.